Processing and Application of Ceramics 11 [3] (2017) 206–212
https://doi.org/10.2298/PAC1703206M

Processing of composites based on NiO, samarium-doped ceria and carbonates (NiO-SDCC) as anode support for solid oxide fuel cells

Lily Siong Mahmud[1,*], Andanastuti Muchtar[1,2,*], Mahendra Rao Somalu[1], Abdul Azim Jais[1]

[1]*Fuel Cell Institute, Universiti Kebangsaan Malaysia, 43600 UKM Bangi, Selangor Darul Ehsan, Malaysia*
[2]*Department of Mechanical and Material Engineering, Faculty of Engineering and Built Environment, Universiti Kebangsaan Malaysia, 43600 UKM Bangi, Selangor Darul Ehsan, Malaysia*

Received 30 December 2016; Received in revised form 23 August 2017; Accepted 8 September 2017

Abstract

NiO-SDCC composites consisting of NiO mixed with Sm-doped ceria (SDC) and carbonates (Li_2CO_3 and Na_2CO_3) were sintered at different temperatures and reduced at 550 °C. The influence of reduction on structure of the NiO-SDCC anode support for solid oxide fuel cells (SOFCs) was investigated. Raman spectra of the NiO-SDCC samples sintered at 500, 600 and 700 °C showed that after reducing at 550 °C NiO was reduced to Ni. In addition, SDC and carbonates (Li_2CO_3 and Na_2CO_3) did not undergo chemical transformation after reduction and were still detected in the samples. However, no Raman modes of carbonates were identified in the NiO-SDCC pellet sintered at 1000 °C and reduced at 550 °C. It is suspected that carbonates were decomposed at high sintering temperature and eliminated due to the reaction between the CO_3^{2-} and hydrogen ions during reduction in humidified gases at 550 °C. The carbonate decomposition increased porosity in the Ni-SDCC pellets and consequently caused formation of brittle and fragile structure unappropriated for SOFC application. Because of that composite NiO-SDC samples without carbonates were also analysed to determine the factors affecting the crack formation. In addition, it was shown that the different reduction temperatures also influenced the microstructure and porosity of the pellets. Thus, it was observed that Ni-SDC pellet reduced at 800 °C has higher electrical conductivity of well-connected microstructures and sufficient porosity than the pellet reduced at 550 °C.

Keywords: *solid oxide fuel cell, NiO-SDCC anode, reduction, structure, electrical conductivity*

I. Introduction

Anode supports are preferred over electrolyte supports in the preparation of solid oxide fuel cells (SOFCs). Cells with anode supports are more advantageous than electrolyte or cathode supported cells due to improved reliability, high stability and reduced electrolyte thickness. The anode supported cells may also significantly reduce the resistance between the electrolyte interfaces [1–3]. Furthermore, high electrical conductivity is mainly considered during the selection of materials suitable for manufacturing SOFC anodes. Material composition, sintering temperature and reduction conditions influence the electrical conductivity of the anode component [2].

* Corresponding author: tel: +603 89213895,
e-mail: *sionglily@gmail.com* (L.S. Mahmud),
e-mail: *muchtar@ukm.edu.my* (A. Muchtar)

Nickel oxide (NiO) is extensively used as a principal anode material because of its chemical stability, high electrical conductivity and high efficiency for both hydrogen oxidation and hydrocarbon fuel reformation [4–6]. Generally, NiO is partially mixed with electrolyte powders, such as yttria-stabilized zirconia (YSZ), scandia-stabilized zirconia (ScSZ), samarium-doped ceria (SDC) and gadolinium-doped ceria (GDC), to form composite anodes of NiO-YSZ [7,8], NiO-ScSZ [9,10], NiO-GDC [11,12], NiO-CGO [5,13] and NiO-SDC [6,14], respectively. Reduction is an important process performed prior to the evaluation of the electrical performance of the anode substrate. Under the reduction conditions, anode cermet, such as NiO-YSZ, is exposed to humidified hydrogen and nitrogen gases at desired temperatures. During reduction, NiO-YSZ is transformed into Ni-YSZ and the metallic Ni phase in Ni-YSZ becomes electrically conductive for effective

electrochemical oxidation at the SOFC anode [4]. Moreover, different reduction temperatures can influence the microstructure and electrochemical properties of an anode, such as in the case of Ni-YSZ anode-supported SOFCs [8].

The characteristics of NiO with ceria-doped electrolytes (e.g., NiO-SDC and NiO-GDC) after reduction have gained significant attention among researchers on SOFCs [5,6]. Only few studies reported the effects of reduction on the properties (such as change in particle sizes and oxygen chemical potential) of the NiO-SDC anode substrate [6,15]. Jarot *et al.* [16] reported that NiO-SDCC (NiO mixed with SDC (samarium-doped ceria) and Li/Na carbonates) can be used as SOFC anode substrate for low-temperature SOFCs. However, the structural characterization of NiO-SDCC as anode-supported SOFCs after reduction has not been reported yet.

In the present study, the influence of reduction on the NiO-SDCC anode structure was studied to determine its reliability for low temperature solid oxide fuel cell (LT-SOFC) application. The presence of carbonates in the NiO-SDCC pellets after reduction was investigated through Raman spectroscopy. This technique was used to investigate the carbonate formation in Ni-based anodes after their exposure to carbon monoxide and determine the existence of nickel sulphide after their exposure to H_2 fuel containing H_2S [17–19]. In addition, the suitability of NiO-SDCC substrate as a support structure of SOFCs was compared with NiO-SDC (sample without carbonates).

II. Experimental

2.1. Preparation

Composites consisting of NiO mixed with SDC (samarium-doped ceria) and carbonates (Li_2CO_3 and Na_2CO_3) were prepared in two steps. Initially, $Sm_{0.2}Ce_{0.8}O_{1.9}$ (Sigma-Aldrich) was mixed with binary carbonates (67 mol% Li_2CO_3 and 33 mol% Na_2CO_3) with a weight ratio of 2 : 1 to form mixture of Sm-doped ceria and carbonates (SDCC). The SDCC mixture was ball milled at 200 rpm for 16 h in ethanol with ZrO_2 balls (with diameter of 5 mm) in a zirconia bowl (250 cm^3) to obtain a homogeneous mixture. The ratio of the powder to ZrO_2 balls was 4 : 1. After milling, the mixture was dried in an oven at 120 °C for 12 h and calcined at 680 °C in static air for 1 h at a heating rate of 10 °C/min. The obtained SDCC powder (40 wt.%) was mixed with NiO powder (60 wt.%) and ball milled under the same conditions applied to the SDCC powder. The powder mixture was subsequently dried in the oven at 90 °C for 24 h prior to its use in the preparation of NiO-SDCC anode pellet.

In the second step, the NiO-SDCC composite powder (85 wt.%) was mixed with polyethylene glycol (PEG, as a binder, Merck) and 15 wt.% of potato starch fine powder used as a pore former. The mixture was ball milled again for 3 h with ethanol and dried at 90 °C for 10 h. The dried powder was ground by using a mortar and pestle, and sieved through a 212 μm woven wire to obtain fine powder. Finally, the powder was dry pressed at 32 MPa into circular pellets with diameter of 25 mm. The approximate thickness of the dry-pressed pellets was less than 1 mm. The pellets were sintered at 500, 600, 700, and 1000 °C in static air for 2 h at a heating rate of 2 °C/min. In addition, NiO-SDC composite samples (with NiO to $Sm_{0.2}Ce_{0.8}O_{1.9}$ weight ratio of 40 : 60 and 15 wt.% of potato starch) were also prepared using the same conditions.

The sintered anode pellets were treated at 550 and 800 °C for 5 h under humidified gases mixture of 10% hydrogen and 90% nitrogen to reduce NiO into Ni.

2.2. Characterization

The anode pellets after sintering and reduction were examined by Raman spectroscopy (Alpha 300R, WITEc Gmbh, Ulm, Germany). The measurement was performed with an excitation wavelength of 488.063 nm. The Raman spectra at each pixel with an imaging area of 4 μm × 4 μm (120 point per line) were obtained at an integration time of 0.1132 s. The Raman images showed the average spectra of areas with identical chemical compositions. Field-emission scanning electron microscope (FESEM, Zeiss Supra-55VP) was used to observe the morphology of the sintered and reduced pellets. Energy-dispersive spectroscopy (EDS) was utilized to determine the elemental composition of the pellets. Porosity of the anode pellets was evaluated using the standard Archimedes method. Phase composition was examined through X-ray diffraction analysis (XRD; Bruker AXS Germany, D8 Advance) using CuKα radiation (λ = 0.15406 nm) with an operating voltage and current of 40 kV and 40 mA, respectively. The scanning range varied between 20° and 80°, with a step size of 0.025° and a counting rate of 0.1 s per scanning step.

2.3. DC electrical conductivity

The DC electrical conductivity of the reduced pellets was determined using the DC 4 point Van Der Pauw method. DC power supply (Keithley 2230-30-1) was utilized to supply current and a digital multimeter (Fluke 8808A) was used to measure the voltage drop across the probes. During the measurement, the samples were maintained under the dry gas mixture of hydrogen (10%) and nitrogen (90%). Conductivity measurements were performed in temperature range from 300 to 800 °C.

III. Results and discussion

3.1. Microstructure of NiO-SDCC

Figure 1 shows the Raman spectra of the NiO-SDCC samples after sintering at 500, 600 and 700 °C and reducing at 550 °C. The peaks of NiO, SDC and carbonates in the Raman spectra of the sintered pellets were

clearly visible. After the reduction, the carbonate peaks in the Raman spectra at 1000–1150 cm^{-1} [20] can also be observed in all three samples. However, it seems that the peak intensity of the samples after the reduction was slightly decreased. Furthermore, the intensive Raman peaks of NiO were observed within 400–510 cm^{-1} in all three samples after the reduction, thereby proving that NiO was not reduced completely to Ni metal at 550 °C. Finally, the SDC peaks for the NiO-SDCC samples after sintering and reduction are observed within 500–664 cm^{-1} and are comparable with those of Raman SDC modes reported in previous study [6].

Figures 2a, 2b and 2c show the morphologies of the NiO-SDCC pellets after sintering at 500, 600, and 700 °C, respectively. After sintering, NiO and SDCC composite grains interact well and are homogenously distributed. The NiO-SDCC pellets sintered at 500, 600 and 700 °C exhibited porosity of 32.8%, 37.6% and 36.6%, respectively. The porosities are satisfactory because the anode support must feature approximately 30–40% porosity to maximize the oxidation reaction [2,21,22].

Figures 3a, 3b and 3c show the morphologies of the Ni-SDCC samples after reduction in the gas mixture of hydrogen and nitrogen at 550 °C. After the reduction, the porosity of the NiO-SDCC pellets (sintered at 500, 600 and 700 °C) slightly increased, in the range of 8–10%. The increased porosity resulted from the reduction of NiO to Ni [23]. Moreover, the carbonates in the reduced pellets sintered at 700 °C started to melt and decompose on the surface of grains (Fig. 3c). This could explain the decreasing of carbonate peak intensity in the Raman spectra of the reduced samples (Fig. 1c).

The NiO-SDCC pellet was also sintered at 1000 °C to investigate the influence of high sintering temperature on the carbonate content in the anode composite. The Raman spectrum of the NiO-SDCC sample sintered at 1000 °C confirms the presence of carbonates (Fig. 4). However, the carbonate peak was not detected in the Raman spectrum of the sample after reduction at 550 °C and only NiO and SDC peaks were found (Fig. 4).

FESEM image of the NiO-SDCC composite sintered at 1000 °C (Fig. 5a) shows that the grain size increases and porosity disappears. The carbonates were expected to melt at high sintering temperatures because their melting temperatures are lower than the applied sintering temperature. The melting points of the lithium carbonate and sodium carbonate are at 727 and 851 °C under static air condition, respectively [24,25]. The melt-

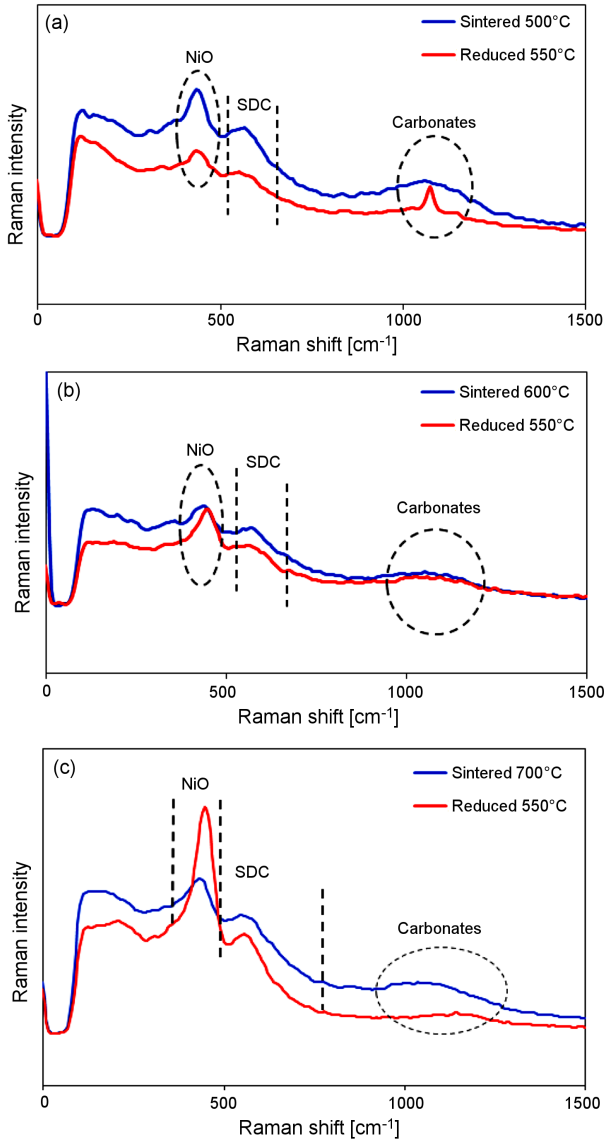

Figure 1. Raman spectra of NiO-SDCC pellets sintered at: a) 500 °C, b) 600 °C and c) 700 °C for 2 h in air before and after reduction at 550 °C for 5 h

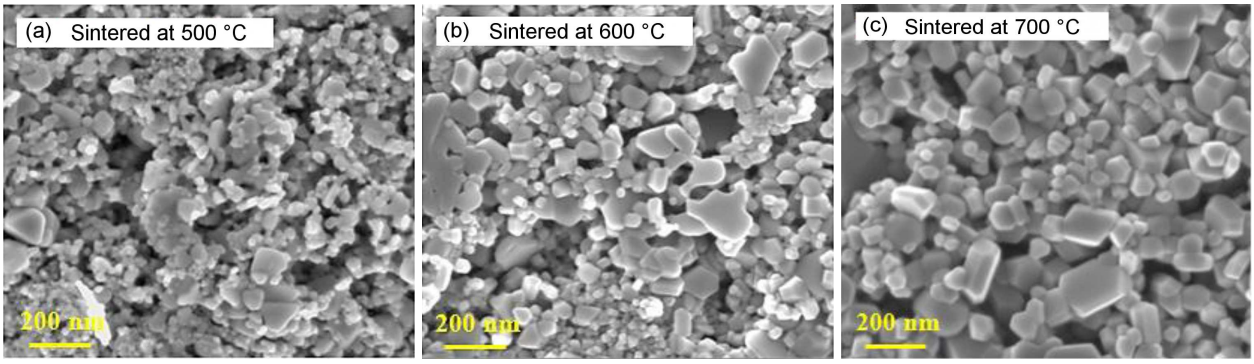

Figure 2. FESEM images of NiO-SDCC pellets after sintering for 2 h at: a) 500 °C, b) 600 °C and c) 700 °C in air

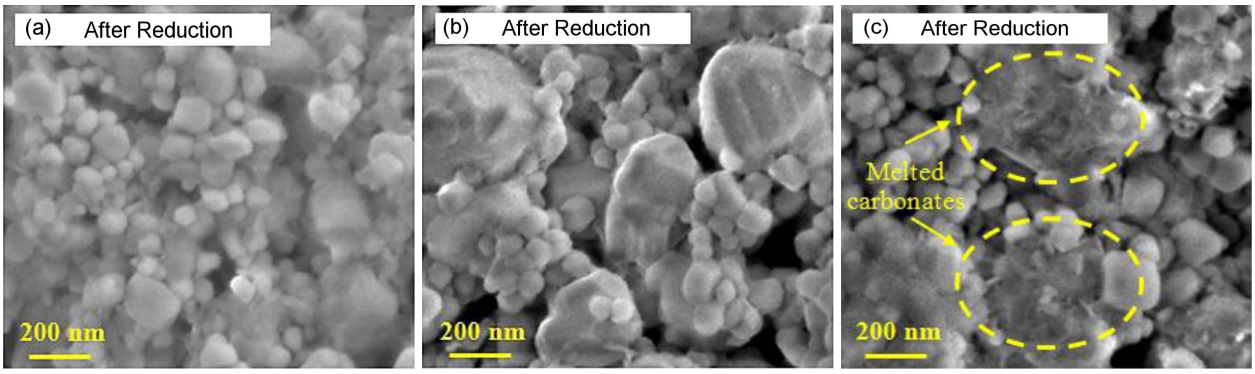

Figure 3. FESEM images of NiO-SDCC pellets after sintering at: a) 500 °C, b) 600 °C and c) 700 °C and reduction at 550 °C

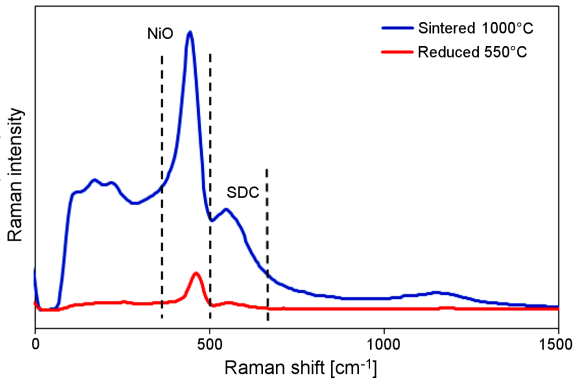

Figure 4. Raman spectra of NiO-SDCC pellet sintered at 1000 °C and reduced at 550 °C

ing temperature of a binary carbonates eutectic for molar ratio of 52 Na_2CO_3 : 48 Li_2CO_3 in the SDC composite is approximately 490 °C [26]. FESEM image of the NiO-SDCC composite sintered at 1000 °C and reduced at 550 °C is shown in Fig. 5b. The residues after carbonate decomposition can be clearly observed on the surface, and they partially filled the pores of the reduced pellets. The carbonates can easily react with hydrogen to form water and carbon dioxide, as shown in Eq. 1 [27]:

$$CO_3^{2-} + 2\,H^+ \longrightarrow CO_2 + H_2O \qquad (1)$$

Thus, the carbonates in the Ni-SDCC anode can be decomposed by the high sintering temperature and the process might be assisted by reaction between carbonate (CO_3^{2-}) and hydrogen ions (H^+) during reduction process. The carbonates disappearance reduced the rigidity of the anode, as shown by the loosely connected particles in Fig. 5b. This was further confirmed with the observation that all the reduced anode pellets easily cracked into pieces after application of a small spring-loaded force onto the sample before the electrical conductivity measurement. Hence, the conductivity of the NiO-SDCC pellets could not be measured in this study.

3.2. Microstructure of NiO-SDC

The composite NiO-SDC samples without carbonates were also analysed to determine the factors affecting the crack formation. The pellets were sintered at 1000 °C and subsequently reduced at two different temperatures (550 and 800 °C). The sintered and reduced NiO-SDC pellets were in good shape with improved rigidity and without any cracks. Figure 6 shows the Raman spectra of the NiO-SDC anode. The Raman spectrum confirmed the presence of SDC with the peaks within the range of 500–664 cm^{-1}. In addition, the intensities of Raman peak of NiO after sintering at 1000 °C and peak of the sample reduced at 550 °C are almost comparable. On the other hand, after the reduction at 800 °C, the intensity of Raman NiO mode decreases remarkably. This condition indicated that NiO was almost completely reduced to Ni metal phase after treatment at 800 °C.

The XRD patterns of the composite NiO-SDC samples (Fig. 7) also showed that NiO was reduced to Ni after treatment at both reduction temperatures (550 and

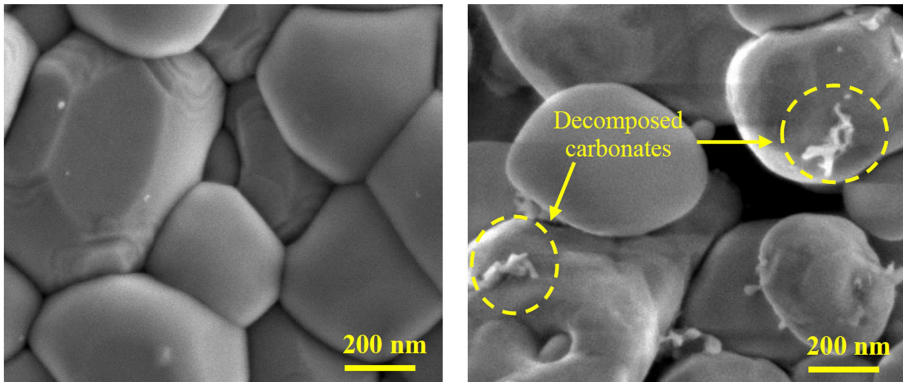

Figure 5. FESEM images of NiO-SDCC pellets: (a) after sintering at 1000 °C for 2 h, and (b) after reduction at 550 °C

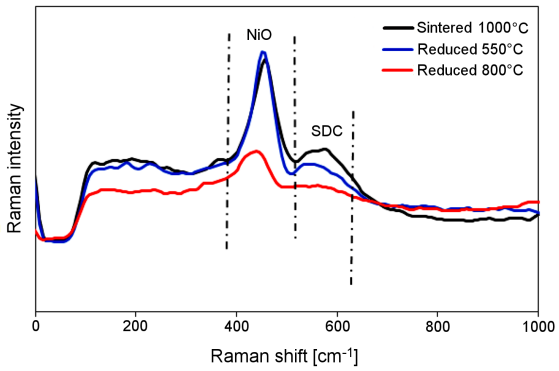

Figure 6. Raman spectra of NiO-SDC pellet sintered at 1000 °C and reduced at 550 °C and 800 °C

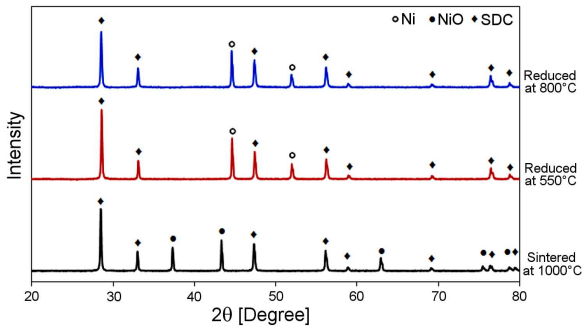

Figure 7. Raman spectra of NiO-SDC pellet sintered at 1000 °C, reduced at 550 °C and 800 °C

800 °C). According to the Raman and XRD results it is justified to claim that the complete reduction of the NiO-SDC can be obtained at 800 °C. Hence, 800 °C was determined as a suitable reduction temperature for the anode. The complete reduction of NiO to Ni is critical for the increase of overall electrical and electrochemical performances of a cell [28].

SEM micrographs and EDS spectra of the NiO-SDC after sintering and reduction are shown in Fig. 8. Figure 8a presents the morphologies of NiO-SDC after sintering at 1000 °C which were dissimilar to those of the sintered NiO-SDCC pellet at the same temperature. Both morphologies of the Ni-SDC after reduction at 550 and 800 °C were different. Microstructures of well-connected particles were observed in the SEM micrograph of the Ni-SDC (Fig. 8c) sample reduced at 800 °C and with acceptable amount of porosity. In comparison with the morphology of the Ni-SDC (Fig. 8b) which was reduced at 550 °C it can be seen that the particles connection was slightly loose in the sample reduced at 800 °C. Figure 8d illustrates the EDS pattern of the NiO-SDC after sintering and Ni content was detected to be 45.1 wt.%. After the reduction the Ni content increased (Figs. 8e,f). The pellets reduced at 550 and 800 °C contain 49.4 and 51.4 wt.% of Ni, respectively. The EDS results are consistent with the Raman observations (Fig. 6), which indicated that the change of NiO into Ni after the reduction at 800 °C was improved.

Porosity of the NiO-SDC pellets after sintering was 44.0%. After reduction at 550 and 800 °C, the porosity of the pellets increased to 60.6% and 57.4%, respectively. Both reduced pellets showed a sufficient porosity, as observed in the FESEM images. Sufficient porosity for anode support is important in transferring fuel gases and improving the DC electrical conductivity of the anode [23,28].

3.3. Conductivity of NiO-SDC

Figure 9 shows the temperature dependence of electrical conductivity of the Ni-SDC pellets reduced at 550 and 800 °C for 5 h. These plots display a positive slope, which proved the predominance of metallic conductivity in the anode and correspond with previous studies [29,30]. However, the Ni-SDC anode pellets reduced

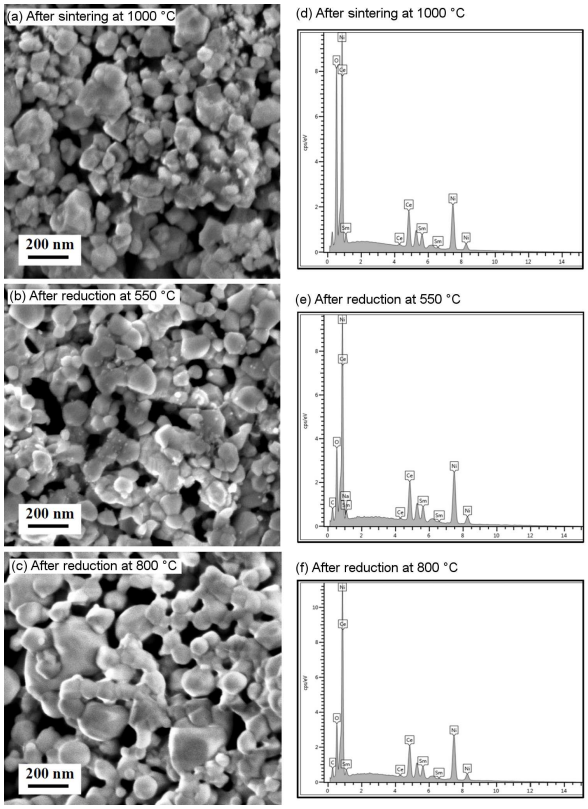

Figure 8. FESEM images and EDS spectrums of NiO-SDC pellets: a,d) after sintering at 1000 °C and after reduction at b,e) 550 °C and c,f) 800 °C for 5 h

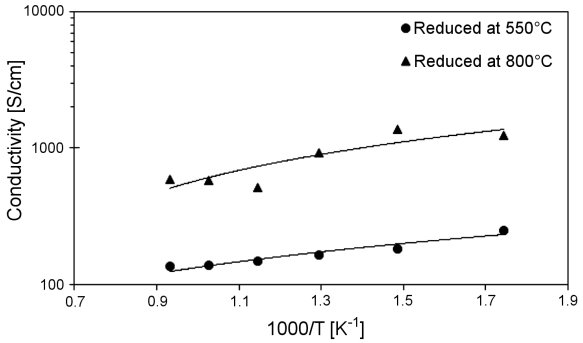

Figure 9. Temperature dependence of the electrical conductivity of Ni-SDC sintered at 1000 °C and subsequently reduced at 550 °C and 800 °C for 5 h

at 550 °C exhibited a lower electrical conductivity than those reduced at 800 °C. The conductivities at 800 °C of the pellets reduced at 550 and 800 °C were 135 and 587 S/cm, respectively. The lower conductivity of the pellets reduced at 550 °C is due to incomplete reduction of NiO to Ni, as confirmed by the Raman analyses. This result further supported the high reliability of Raman and XRD in determining the optimum reduction temperature. Moreover, a similar result was shown in the case of Ni-YSZ anode pellets, where the electrical conductivity of the anode was improved by a factor of approximately 6 upon reduction at 1000 °C compared with that at 650 °C [31]. Therefore, this study revealed that the particle connectivity and suitable reduction temperature are also critical parameters in increasing the electrical conductivity and porosity of anode component.

IV. Conclusions

NiO-SDCC composites consisting of NiO mixed with Sm-doped ceria (SDC) and carbonates (Li_2CO_3 and Na_2CO_3) were sintered at different temperatures and reduced at 550 °C. Raman spectroscopy was applied to identify the presence of carbonates in NiO-SDCC after sintering and reduction. This technique was also applied to investigate the change in NiO to Ni phase after reduction. Carbonates were decomposed at high sintering temperatures, especially at temperature higher than 700 °C, and by hydrogen during the reduction. The carbonate decomposition increased the porosity and decreased the rigidity of NiO-SDCC anode pellets. Therefore, NiO-SDCC pellets are unsuitable as supporting structures of a single cell compared with those of NiO-SDC pellets sintered at 1000 °C. The sintered NiO-SDC pellets were rigid, and they showed no fracture after reduction. The NiO-SDC pellets reduced at 550 °C also showed lower electrical conductivity than those reduced at 800 °C. This result proved that 550 °C is an insufficient temperature for the complete reduction of NiO to Ni, as supported by a low intensity peak in Raman spectrum. Thus, it can be concluded that the NiO-SDC combined with the SDCC electrolyte film is recommended in SOFC fabrication.

Acknowledgements: This work was supported by the Universiti Kebangsaan Malaysia (UKM) and the Ministry of Science, Technology and Innovation, Malaysia through research grants 03-01-02-SF1079 and FRGS/2/2013/TK06/UKM/02/9. The authors would like to acknowledge the support of the Centre for Research and Instrumentation Management, UKM for providing excellent testing equipment. The first author would also like to acknowledge the Malaysian Ministry of Higher Education for supporting her graduate studies.

References

1. V. Haanappel, "Advances in solid oxide fuel cell development between 1995 and 2010 at Forschungszentrum Jülich GmbH, Germany", pp. 247–274 in *Fuel Cell Science and Engineering*. Eds. by D. Stolten, B. Emonts, 2012.
2. K. Huang, J.B. Goodenough, *Solid Oxide Fuel Cell Technology: Principles, Performance and Operations*, Woodhead Publishing Limited and CRC Press LLC, Cambridge, UK 2009.
3. S. Bozorgmehri, M. Hamedi, "Analysis of design parameters in anode-supported solid oxide fuel cells using response surface methodology", *Fuel Cells*, **13** [5] (2013) 751–760.
4. J.W. Fergus, R. Hui, X. Li, D.P. Wilkinson, J. Zhang, *Solid Oxide Fuel Cells: Materials Properties and Performance*, CRC Press, Taylor & Francis Group, UK 2009.
5. R.C. Maher, P.R. Shearing, E. Brightman, D.J.L. Brett, N.P. Brandon, L.F. Cohen, "Reduction dynamics of doped ceria, nickel oxide, and cermet composites probed using in situ Raman spectroscopy", *Adv. Sci.*, **3** [1] (2016) 1–8.
6. T. Matsui, K. Eguchi, T. Furukawa, T. Okanishi, H. Muroyama, K. Eguchi, "In-operando Raman spectroscopy study on oxygen chemical potential gradient in Ni-SDC cermet anode for SOFCs", *ECS Transactions*, **68** [1] (2015) 1083–1090.
7. Z. Cheng, M. Liu, "Characterization of sulfur poisoning of Ni-YSZ anodes for solid oxide fuel cells using in situ Raman microspectroscopy", *Solid State Ionics*, **178** [13-14] (2007) 925–935.
8. T.S. Li, W.G. Wang, H. Miao, T. Chen, C. Xu, "Effect of reduction temperature on the electrochemical properties of a Ni/YSZ anode-supported solid oxide fuel cell", *J. Alloys Compd.*, **495** [1] (2010) 138–143.
9. M.R. Somalu, N.P. Brandon, "Rheological studies of nickel/scandia-stabilized-zirconia screen printing inks for solid oxide fuel cell anode fabrication", *J. Am. Ceram. Soc.*, **95** [4] (2012) 1220–1228.
10. D.A. Agarkov, I.N. Burmistrov, F.M. Tsybrov, Tartakovskii, II, V.V. Kharton, S.I. Bredikhin, "Kinetics of NiO reduction and morphological changes in composite anodes of solid oxide fuel cells: Estimate using Raman scattering technique", *Russ. J. Electrochem.*, **52** [7] (2016) 600–605.
11. C. Fu, S. H. Chan, Q. Liu, X. Ge, G. Pasciak, "Fabrication and evaluation of Ni-GDC composite anode prepared by aqueous-based tape casting method for low-temperature solid oxide fuel cell", *Int. J. Hydrogen Energy*, **35** [1] (2010) 301–307.
12. H. Choi, G. Cho, S.-W. Cha, "Fabrication and characterization of anode supported YSZ/GDC bilayer electrolyte SOFC using dry press process", *Int. J. Precis. Eng. Manuf.*, **1** [2] (2014) 95–99.
13. S.P.S. Shaikh, A. Muchtar, M.R. Somalu, "A review on the selection of anode materials for solid-oxide fuel cells", *Renew. Sust. Energy Rev.*, **51** (2015) 1–8.
14. M. Chen, B.H. Kim, Q. Xu, B.G. Ahn, D.P. Huang, "Fabrication and performance of anode-supported solid oxide fuel cells via slurry spin coating", *J. Membr. Sci.*, **360** [1-2] (2010) 461–468.
15. K. Sugihara, M. Asamoto, Y. Itagaki, T. Takemasa, S. Yamaguchi, Y. Sadaoka, H. Yahiro, "A quantitative analysis of influence of Ni particle size of SDC-supported anode on SOFC performance: Effect of particle size of SDC support", *Solid State Ionics*, **262** (2014) 433–437.
16. R. Jarot, A. Muchtar, W.R. Wan Daud, M. Norhamidi, E.H. Majlan, "Porous NiO-SDC carbonates composite anode

for LT-SOFC applications produced by pressureless sintering", *Appl. Mech. Mater.*, **52** (2011) 488–493.
17. R.C. Maher, V. Duboviks, G.J. Offer, M. Kishimoto, N.P. Brandon, L.F. Cohen, "Raman spectroscopy of solid oxide fuel cells: Technique overview and application to carbon deposition analysis", *Fuel Cells*, **13** [4] (2013) 455–469.
18. J. Dong, Z. Cheng, S. Zha, M. Liu, "Identification of nickel sulfides on Ni-YSZ cermet exposed to H_2 fuel containing H_2S using Raman spectroscopy", *J. Power Sources*, **156** [2] (2006) 461–465.
19. L. Zhao, J. Zhang, T. Becker, S.P. Jiang, "Raman spectroscopy study of chromium deposition on $La_{0.6}Sr_{0.4}Co_{0.2}Fe_{0.8}O_{3-\delta}$ cathode of solid oxide fuel cells", *J. Electrochem. Soc.*, **161** [6] (2014) F687–F693.
20. N.P. McKay, D.L. Dettman, R.T. Downs, J.T. Overpeck, "On the potential of Raman-spectroscopy-based carbonate mass spectrometry", *J. Raman Spectrosc.*, **44** [3] (2013) 469–474.
21. N. Oishi, A. Atkinson, N.P. Brandon, J.A. Kilner, B.C.H. Steele, "Fabrication of an anode-supported gadolinium-doped ceria solid oxide fuel cell and its operation at 550 °C", *J. Am. Ceram. Soc.*, **88** [6] (2005) 1394–1396.
22. M. Kim, J. Lee, J.-H. Han, "Fabrication of anode support for solid oxide fuel cell using zirconium hydroxide as a pore former", *J. Power Sources*, **196** [5] (2011) 2475–2482.
23. F. Zhao, A.V. Virkar, "Dependence of polarization in anode-supported solid oxide fuel cells on various cell parameters", *J. Power Sources*, **141** [1] (2005) 79–95.
24. F. Senese, *Introduction to Inorganic Chemistry*, Frostburg State University MD, USA, 2010.
25. A. Timoshevskii, M. Ktalkherman, V. Emel'Kin, B. Pozdnyakov, A. Zamyatin, "High-temperature decomposition of lithium carbonate at atmospheric pressure", *High Temp.*, **46** [3] (2008) 414–421.
26. M. Chen, H. Zhang, L. Fan, C. Wang, B. Zhu, "Ceria-carbonate composite for low temperature solid oxide fuel cell: Sintering aid and composite effect", *Int. J. Hydrogen Energy*, **39** [23] (2014) 12309–12316.
27. J. Clark, *Reactions of the Hexaaqua Ions with Carbonate Ions*, University of California, USA, 2014.
28. S.-W. Cheng, C.-H. Tsai, S.-H. Wu, C.-K. Liu, Y.-N. Cheng, R.-Y. Lee, "Effects of reduction process on the electrochemical and microstructural properties for electrolyte-supported SOFC", *Int. J. Hydrogen Energy*, **40** [3] (2015) 1534–1540.
29. J.H. Yu, G.W. Park, S. Lee, S.K. Woo, "Microstructural effects on the electrical and mechanical properties of Ni-YSZ cermet for SOFC anode", *J. Power Sources*, **163** [2] (2007) 926–932.
30. M.R. Somalu, V. Yufit, D. Cumming, E. Lorente, N.P. Brandon, "Fabrication and characterization of Ni/ScSZ cermet anodes for IT-SOFCs", *Int. J. Hydrogen Energy*, **36** [9] (2011) 5557–5566.
31. L. Grahl-Madsen, P.H. Larsen, N. Bonanos, J. Engell, S. Linderoth, "Mechanical strength and electrical conductivity of Ni-YSZ cermets fabricated by viscous processing", *J. Mater. Sci.*, **41** [4] (2006) 1097–1107.